SCIENTIFIC REPORTS

OPEN

Received: 25 August 2015
Accepted: 11 January 2016
Published: 16 February 2016

Post-illumination activity of SnO_2 nanoparticle-decorated Cu_2O nanocubes by H_2O_2 production in dark from photocatalytic "memory"

Lingmei Liu[1], Wuzhu Sun[1], Weiyi Yang[1], Qi Li[1,†] & Jian Ku Shang[2]

Most photocatalysts only function under illumination, while many potential applications require continuous activities in dark. Thus, novel photocatalysts should be developed, which could store part of their photoactivity in "memory" under illumination and then be active from this "memory" after the illumination is turned off for an extended period of time. Here a novel composite photocatalyst of SnO_2 nanoparticle-decorated Cu_2O nanocubes is developed. Their large conduction band potential difference and the inner electrostatic field formed in the *p-n* heterojunction provide a strong driving force for photogenerated electrons to move from Cu_2O to SnO_2 under visible light illumination, which could then be released to react with O_2 in dark to produce H_2O_2 for its post-illumination activity. This work demonstrates that the selection of decoration components for photocatalysts with the post-illumination photocatalytic "memory" could be largely expanded to semiconductors with conduction band potentials less positive than the two-electron reduction potential of O_2.

Over the past a few decades, semiconductor-based photocatalysts have been widely explored for both solar energy conversion and environmental applications[1–5]. It is generally recognized that various reactive oxygen species (ROSs) could be produced by photocatalysts *in situ* under proper illumination to disinfect microorganisms and degrade organic pollutants at ambient temperature and pressure[6–9]. Most of these photocatalysts only functioned under illumination because their production of ROSs relied on continuous illumination to generate electron-hole pairs[10,11]. However, many potential applications require the continuous activity in the dark for an extended period of time. For example, nosocomial infection by microorganism transmit in hospitals is among the top death causes in many countries, which could be controlled by creating self-disinfection environment in hospitals[12,13]. Thus, if a photocatalyst could store part of its photoactivity in "memory" under visible light illumination and then be active from this "memory" after the illumination is turned off for an extended period of time, it could provide continuous solar-powered disinfection during daytime and at night to save lives with a high efficiency and relatively low cost/energy consumption.

Recently, an interesting post-illumination photocatalytic "memory" effect was found in several photocatalytic material systems, which could be active in the dark after the illumination was switched off[14–19]. For single-crystalline Se nanorods[17] and semimetal Bi nanoparticles[18], a few charge carriers were found to remain at their surfaces and participate in the $^{\bullet}OH$ production for their activity after the cease of illumination, and their activity in the dark could last no longer than 0.5 h due to the very limited charge carrier amount. For TiON/PdO[14,15], Cu_2O-NS/TiO_2-NI[16], and I-TiO_2[19], however, photogenerated electrons could transfer from the light absorber component to the decoration component, be trapped, and then be released to react with O_2 in the environment to produce $^{\bullet}O_2^-$ when the light illumination was turned off. $^{\bullet}O_2^-$ could subsequently react with H_2O to

[1]Environment Functional Materials Division, Shenyang National Laboratory for Materials Science, Institute of Metal Research, Chinese Academy of Sciences, Shenyang 110016, P. R. China. [2]Department of Materials Science and Engineering, University of Illinois at Urbana-Champaign, Urbana, Illinois 61801, USA. [†]Present address: 72 Wenhua Road, Shenyang, Liaoning Province, 110016, P. R. China. Correspondence and requests for materials should be addressed to Q.L. (email: qili@imr.ac.cn)

produce $^{\bullet}OH$. Due to the gradual release of trapped photogenerated electrons, their activity in dark could last for more than 10 h, which is desirable for the construction of continuous solar-powered photocatalytic disinfection/degradation systems effective for both daytime and at night.

It is generally believed that the redox ability of photogenerated electrons and holes highly relied on the conduction and valence band potentials of the photocatalyst[20]. The one-, two-, and four-electron reduction potentials of O_2 could be expressed as reactions (1) to (3) as following[8]:

$$e^- + O_2 \rightarrow {}^{\bullet}O_2^- \quad (1)$$

$$2e^- + O_2 + 2H^+ \rightarrow H_2O_2 \quad (2)$$

$$4e^- + O_2 + 4H^+ \rightarrow 2H_2O \quad (3)$$

Till now, photocatalysts with the post-illumination photocatalytic "memory" effect required that photogenerated electrons were trapped on decoration components with the conduction band potential negative than the one-electron reduction potential of O_2 (−0.05 V vs NHE (Normal Hydrogen Electrode)) to react with O_2 in the dark to produce $^{\bullet}O_2^-$ and subsequently $^{\bullet}OH$, which largely limited the selection of decoration components. Their relatively more negative conduction band potentials also lowered the potential difference between their conduction bands and that of the light absorber components. Thus, it would be interesting to examine if a decoration component with the conduction band potential less positive than the two-electron reduction potential of O_2 (0.68 V vs NHE) could be effective to generate activity from the production of H_2O_2 in the dark, which could not only largely expand the the selection of potential decoration components but also increase the conduction band potential difference to enhance the driving force for the photogenerated electrons to be injected from the light absorber component's conduction band to that of the decoration component for their better transfer, trapping and subsequent release.

As an *n*-type, wide band gap semiconductor with interesting chemical, physical and mechanical properties, tin dioxide (SnO_2) had been extensively studied for applications in gas sensors, dye-based solar cells, transparent conducting electrodes, and catalyst supports[21,22]. The chemical state of Sn could exchange between $Sn^{2+}$and $Sn^{4+}$by trapping and release electrons, while it has a conduction band potential (0.4 V vs NHE) less positive than the two-electron reduction potential of O_2[22,23]. Thus, it could have the potential to serve as the decoration component in a composite photocatalyst system to trap the photogenerated electrons injected from the light absorber component, and release them in the dark by the reaction with O_2 to produce active H_2O_2 to possess the post-illumination photocatalytic "memory" effect. In this work, we designed a novel Cu_2O/SnO_2 composite photocatalyst composed of Cu_2O nanocubes decorated with SnO_2 nanoparticles (Cu_2O/SnO_2), in which Cu_2O nanocubes served as the main light absorption component for a good visible light absorption capability while SnO_2 nanoparticles formed *p-n* heterojunctions of good contact with Cu_2O nanocubes to serve as the decoration component. The large potential difference (~1.5 eV) between the conduction bands of Cu_2O and SnO_2[23], combined with the inner electrostatic field ξ formed in the *p-n* heterojunction, provided a strong driving force for the photogenerated electrons to move from Cu_2O to SnO_2 through the heterojunction, which resulted in the enhanced photocatalytic performance under visible light illumination from better charge-carrier separation. The post-illumination photocatalytic "memory" effect was observed as expected for this composite Cu_2O/SnO_2 photocatalyst, and the working mechanism was verified as the production of H_2O_2 by the release of trapped photogenerated electrons from SnO_2 to react with O_2 in the dark.

Results

The formation and morphology of SnO_2 nanoparticle-decorated Cu_2O nanocubes. The electron-hole pair recombination could be largely reduced in single crystal photocatalysts because they have much fewer defects compared with their polycrystalline counterparts, where the electron-hole pair recombination tends to occur[24]. Figure 1a shows the TEM image of the as-prepared Cu_2O sample and the insert in Fig. 1a shows the corresponding selected area electron diffraction (SAED) pattern. It clearly demonstrated that the sample was composed of desirable single crystal nanocubes, which would favor the transportation of photogenerated electrons/holes and was ideal for constructing heterojunctions with SnO_2 nanoparticles in our material design. The average edge length of these Cu_2O nanocubes was ~70 nm, and all their six exposed surfaces were {100} facets. Their fine nanosize could largely increase their specific surface area compared with their counterparts with submicron sizes[25], beneficial to their contact efficiency with pollutants in water.

The control of the hydrolytic speed of tin precursors was critical for the formation of uniformly dispersed SnO_2 nanoparticles on these Cu_2O nanocubes. In our approach, ethyl acetate ($C_4H_8O_2$) was chosen as the hydrolysis agent to get a good dispersion of SnO_2 nanoparticles onto the Cu_2O nanocube surface. As shown in Fig. 1b, the Cu_2O nanocube morphology was well preserved after the deposition and subsequent hydrothermal process to decorate SnO_2 nanoparticles onto the Cu_2O nanocube surface and their crystallization. The surfaces of Cu_2O nanocubes became relatively rough after the SnO_2 nanoparticle decoration. Figure 1c shows the TEM image of SnO_2 nanoparticle-decorated Cu_2O nanocubes with a higher magnification. It demonstrated clearly that fine SnO_2 nanoparticles distributed uniformly on surfaces of Cu_2O nanocubes, and their average size was ~5 nm.

Figure 1d shows a representative HRTEM image of the Cu_2O/SnO_2 interface area on these SnO_2 nanoparticle-decorated Cu_2O nanocubes. The HRTEM image of the SnO_2 nanoparticle area verified their highly crystallized structure. One set of lattice planes could be clearly observed with the *d*-spacing at ~0.34 nm, corresponding to the (101) plane of the tetragonal rutile structure of SnO_2 phase. The HRTEM image of the Cu_2O nanocube area also verified its highly crystallized structure. The electron beam was aligned along [001] direction,

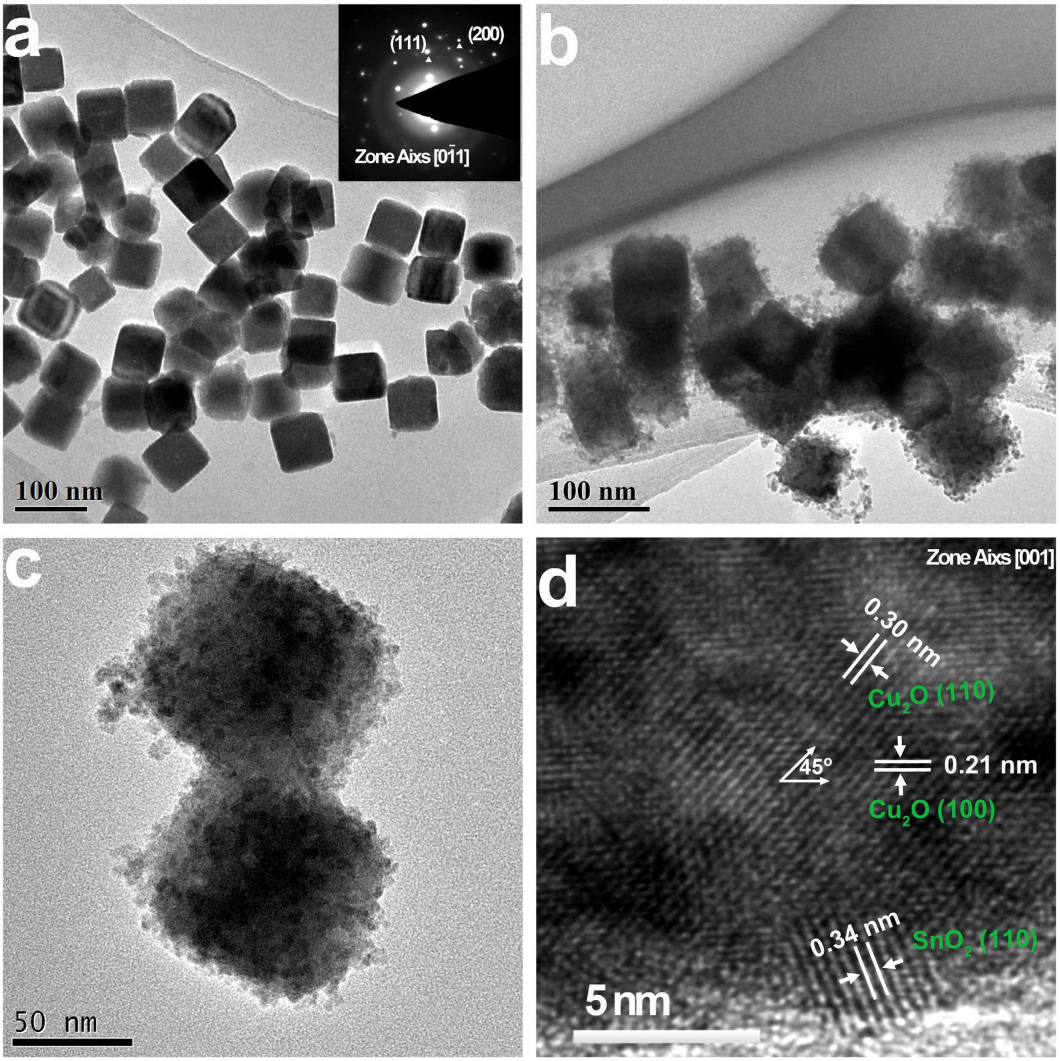

Figure 1. (**a**) The TEM image of the as-prepared Cu_2O sample. (Note, insert plot in Fig. 1a shows its corresponding selected area electron diffraction pattern.) (**b**) and (**c**) TEM images of Cu_2O nanocubes decorated with SnO_2 nanoparticles. (**d**) HRTEM image of the Cu_2O/SnO_2 interface area.

two sets of lattice planes could be clearly observed with the *d*-spacing at ~0.30 nm and ~0.21 nm, respectively, and their separation angle was ~45°, corresponding to the (110) and (100) planes of the fcc Cu_2O phase. The good crystallization of both Cu_2O nanocubes and SnO_2 nanoparticles was beneficial to a good photocatalytic performance due to their lack of defects. The observed Cu_2O/SnO_2 interface indicated that these SnO_2 nanoparticles grew on Cu_2O nanocubes through our synthesis approach and *p-n* heterojunctions were formed with good contact between *p*-type Cu_2O and *n*-type SnO_2, beneficial to the photoexcited electron transfer between them.

Crystal structure and chemical composition of SnO_2 nanoparticle-decorated Cu_2O nanocubes. Figure 2a shows the X-ray diffraction pattern of as-synthesized Cu_2O nanocubes, compared with that of SnO_2 nanoparticle-decorated Cu_2O nanocubes. For both samples, no diffraction peaks of CuO or Cu could be detected. All diffraction peaks in curve a belonged to the fcc Cu_2O phase (PDF Card No. 05-0667), and the strong and sharp peaks indicated that these Cu_2O nanocubes had a high degree of crystallinity. After the decoration with SnO_2 nanoparticles, several new diffraction peaks emerged in curve b, which could be readily indexed to tetragonal rutile structure of SnO_2 (PDF Card No. 41-1445). These peaks had relatively weak intensities due to the much smaller size of SnO_2 nanoparticles, compared with Cu_2O nanocubes. No other diffraction peak could be observed, which confirmed that the final product was composed of Cu_2O and SnO_2. The amount of SnO_2 nanoparticles in the Cu_2O/SnO_2 sample was measured by the sodium diethydlthiocabamate spectrophotometric method, and SnO_2:Cu_2O molar ratio was determined at ~0.15: 1.

The chemical composition and element valence states in SnO_2 nanoparticle-decorated Cu_2O nanocubes were investigated by X-ray photoelectron spectroscopy (XPS). Figure 2b shows the XPS survey spectrum of the Cu_2O/SnO_2 sample, which demonstrated clearly the existence of Sn, O, and Cu in the sample. Due to the widespread presence of carbon in the environment, C *1s* peak could also be observed in the XPS survey spectrum. Figure 2c shows the high resolution XPS spectrum over Cu $2p_{3/2}$ peak. The main peak located at 932.7 eV could be attributed

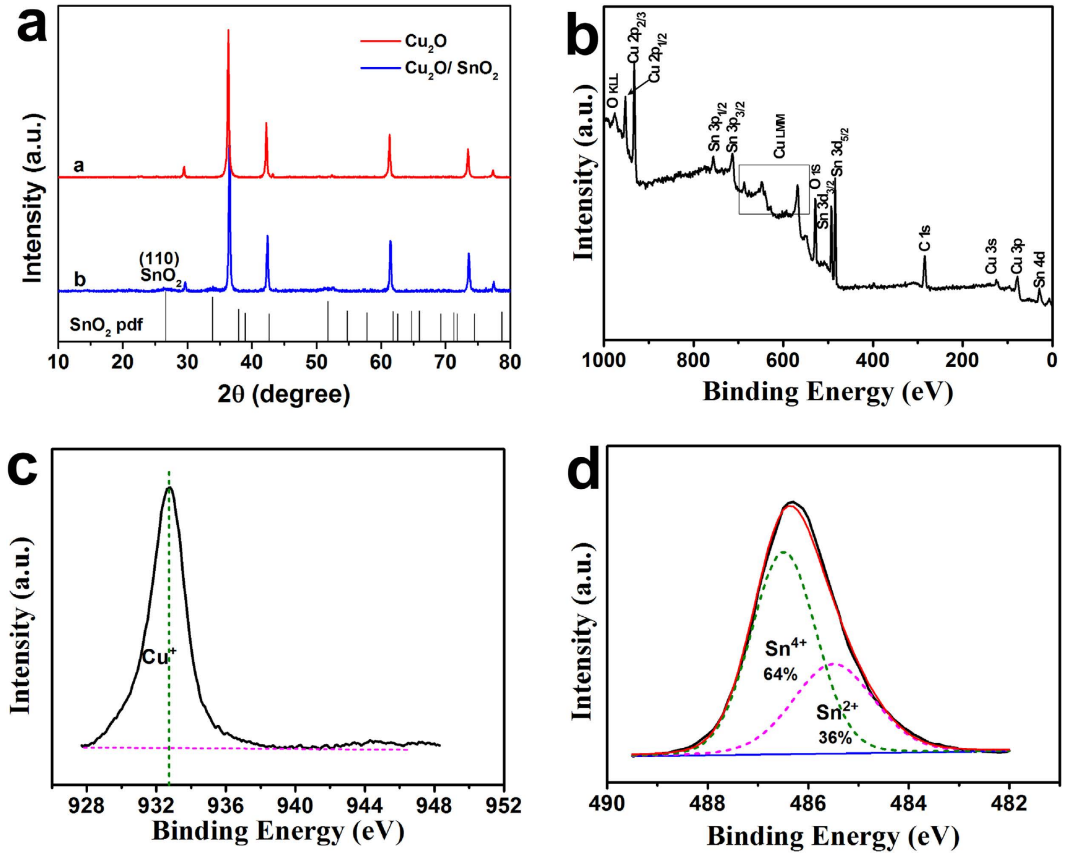

Figure 2. (**a**) X-ray diffraction pattern of as-synthesized Cu_2O nanocubes, compared with that of SnO_2 nanoparticle-decorated Cu_2O nanocubes. (**b**) XPS survey spectrum of the Cu_2O/SnO_2 sample. (**c**) and (**d**) High resolution XPS spectrum over Cu $2p_{3/2}$ peak and Sn $3d_{5/2}$ peak, respectively.

to the Cu^+ $2p_{3/2}$ orbitals[25]. No obvious shake-up satellite peaks on the higher binding energy side could observed, which confirmed no existence of Cu^{2+}on the sample surface[26,27]. Figure 2d shows the high-resolution XPS spectrum over Sn $3d_{5/2}$ peak. It could be best fitted by the combination of two peaks centered at 486.5 eV and 485.5 eV, which could be assigned to $Sn^{4+}3d_{5/2}$ peak and $Sn^{2+}3d_{5/2}$ peak, respectively[28,29]. Thus, a small portion of Sn^{4+}on the SnO_2 nanoparticle surface was reduced to Sn^{2+}during the sample synthesis and storage under normal ambient condition. The Sn^{2+}percentage was determined to be ~36%, while no SnO could be distinguished either in TEM or XRD analysis results. As a surface characterization technique, XPS could determine the surface composition within a very shallow depth. Thus, the existence of Sn^{2+}must be on the very surface of SnO_2 nanoparticles, while the dominant Sn species in the sample existed as Sn^{4+}. It had been well reported in literature that Sn^{2+}state could be detected on the surface of SnO_2 nanoparticles due to the oxygen deficiency at the surface of SnO_2[28,29].

Optical properties of SnO_2 nanoparticle-decorated Cu_2O nanocubes. The optical properties of SnO_2 nanoparticle-decorated Cu_2O nanocubes were investigated by measuring their diffuse reflectance spectrum. From the reflectance data, optical absorbance could be approximated by the Kubelka-Munk function, as given by Eq. (4):

$$F(R) = \frac{(1 - R)^2}{2R} \tag{4}$$

where R is the diffuse reflectance[30]. Figure 3a shows the light absorbance (in term of Kubelka-Munk equivalent absorbance units) of the Cu_2O/SnO_2 sample, compared with that of the as-synthesized Cu_2O nanocubes and SnO_2 nanoparticles. SnO_2 nanoparticles demonstrated the characteristic spectrum with the fundamental absorbance stopping edge at ~350 nm, so most of their adsorption was within the UV light region[23]. Cu_2O nanocubes, however, demonstrated a largely enhanced light absorption in the visible light region. Their absorbance stopping edge was found at ~600 nm, which was in accordance with the reported band gap of Cu_2O at ~2.1 eV[31]. Light absorbance shoulder peaks and tail in the red and near IR regions were observed on the light absorbance spectrum of Cu_2O nanocubes, which could be attributed to their light scattering from their cubic morphology[32,33]. After being decorated with SnO_2 nanoparticles, the light absorbance behavior of the Cu_2O/SnO_2 sample maintained most characteristics of Cu_2O nanocubes because Cu_2O was its major component, while the interface charge transfer (IFCT) from SnO_2 VB to Cu_2O led to the occurrence of other shoulder peaks[34]. This observation further

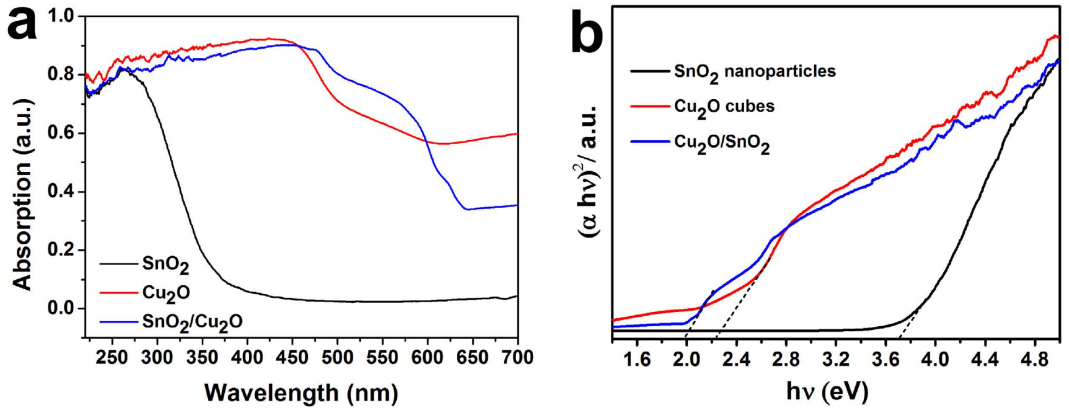

Figure 3. (**a**) The light absorbance (in term of Kubelka-Munk equivalent absorbance units) of the Cu_2O/SnO_2 sample, compared with that of the as-synthesized Cu_2O nanocubes and SnO_2 nanoparticles. (**b**) Tauc Plots ($((F(R)*hv)^n$ vs hv) constructed from Fig. 3a.

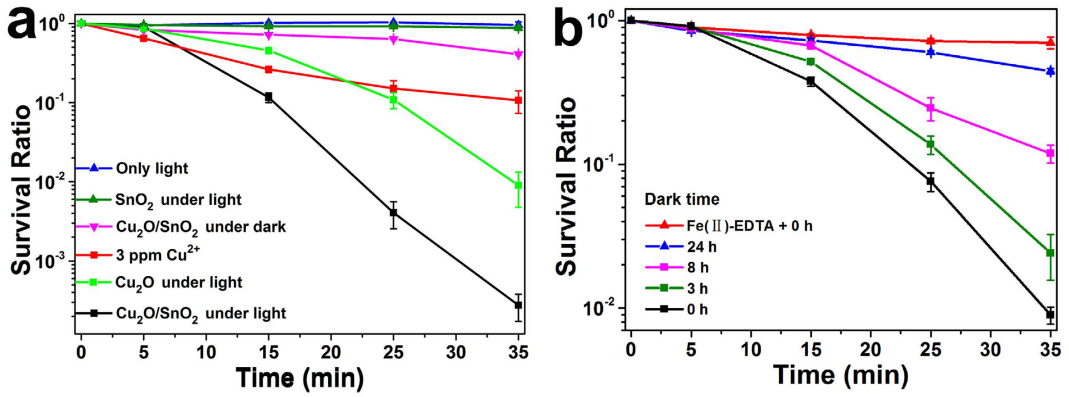

Figure 4. (**a**) The survival ratio of S. aureus cells with the treatment by the Cu_2O/SnO_2 sample under visible light illumination, compared with that without photocatalyst under visible light illumination, that by the Cu2O/SnO_2 sample in the dark, that by SnO_2 nanoparticles under visible light illumination, that by Cu_2O nanocubes under visible light illumination, and that by Cu^{2+} ion with 3 ppm concentration. (**b**) The *S. aureus* cell survival ratios in the dark treated by pre-illuminated Cu_2O/SnO_2 samples after being stored in the dark for various times, compared with that with a H_2O_2 scavenger, EDTA-Fe(II) (0.1 M), in the *S. aureus* cell suspension treated by the pre-illuminated Cu_2O/SnO_2 sample in the dark with the dark storage time of 0 h.

confirmed the formation of heterojunctions between Cu_2O and SnO_2 in this sample. The band gap values of these three photocatalyst samples were determined by the construction of Tauc Plots ($((F(R)*hv)^n$ vs hv) from their light absorbance data[35]. Figure 3b shows Tauc Plots of these three photocatalyst samples, respectively. As direct band gap semiconductors, n should be taken as 2 for both Cu_2O and SnO_2[31,35]. Thus, the extrapolation of the linear region to the photon energy axis could yield their bandgap values of ~3.71 eV for SnO_2 nanoparticles, ~2.27 eV for Cu_2O nanocubes and ~2.16 eV for the Cu_2O/SnO_2 sample, consistent with their light absorption performances.

Photocatalytic disinfection of *Staphylococcus aureus* bacteria under visible light illumination. The superior photocatalytic performance of SnO_2 nanoparticle-decorated Cu_2O nanocubes was demonstrated by their photocatalytic disinfection effect on the viability of *S. aureus* cells, which is a common pathogenic coccus that could cause nonspecific infection and nosocomial infection[13,36]. The photocatalytic disinfection was conducted by exposing *S. aureus* cells suspended in 0.9% NaCl solution with the photocatalyst under visible light illumination for varying time intervals. The survival ratio of *S. aureus* was determined by the ratio of N_t/N_0, where N_0 and N_t were the numbers of colony-forming units at the initial and each following time interval, respectively. Figure 4a shows the survival ratio of *S. aureus* cells under different treatment conditions. When no photocatalyst was present, no obvious change was observed for the survival ratio of *S. aureus* cells under visible light illumination, which suggested that visible light itself could not disinfect *S. aureus* cells. SnO_2 nanoparticles also did not show an obvious bactericidal effect under visible light illumination because they could not be activated by visible light due to their wide band gap of ~3.71 eV. Cu_2O nanocubes demonstrated an obvious bactericidal effect under visible light illumination. After 35 min treatment, the survival ratio of *S. aureus* cells dropped to ~10^{-2}, which could be mainly attributed to their strong visible light absorption (band gap of ~2.27) and subsequent photocatalytic activity under visible light illumination. For the Cu_2O/SnO_2 sample, it only showed a moderate bactericidal

effect on *S. aureus* cells without light illumination. After 35 min treatment, the survival ratio of *S. aureus* cells was still ~40.8%, which should come from the well-known bactericidal effect of copper-based oxides. The detailed discussion of Cu ion leakage from the Cu_2O/SnO_2 sample during the treatment process and its minor contribution to the disinfection of *S. aureus* cells can be found in the supplementary information. Under visible light illumination, however, the Cu_2O/SnO_2 sample demonstrated a much faster bactericidal effect on *S. aureus* cells. After a relatively slow dropping for the first 5 min of the treatment, the survival ratio of *S. aureus* cells dropped sharply and continuously with the increase of the treatment time. The survival ratio of *S. aureus* cells dropped to ~$2.78*10^{-4}$ after only 35 min treatment, more than 3 magnitudes lower than that without visible light illumination. From the comparison, it is clear that the demonstrated superior bactericidal effect of SnO_2 nanoparticle-decorated Cu_2O nanocubes on *S. aureus* cells under visible light illumination could be mainly attributed to their superior photocatalytic disinfection performance, not the modest bactericidal effect from the Cu_2O nanocubes itself in this composite photocatalyst system. The formation of *p-n* heterojunctions Cu_2O and SnO_2 could largely enhance the charge carrier separation, which resulted in the largely enhanced photocatalytic *S. aureus* cell disinfection performance of the Cu_2O/SnO_2 sample, compared with pure Cu_2O nanocubes. To further demonstrate the superior photocatalytic performance of the Cu_2O/SnO_2 sample, its photocatalytic degradation effect on an antibiotic sulfamethoxazole (SMX) was also examined under visible light illumination, and the results can be found in the supplementary information.

Post-illumination photocatalytic "memory" disinfection of *Staphylococcus aureus* bacteria in the dark. As expected, the post-illumination photocatalytic "memory" disinfection of *S. aureus* cells in the dark was observed for SnO_2 nanoparticle-decorated Cu_2O nanocubes. In this experiment series, Cu_2O/SnO_2 samples were firstly illuminated by the same visible light source used in the photocatalytic disinfection experiment for ~3 h. Then, the visible light was shut off and the samples were stored in a dark environment for 0 h, 3 h, 8 h, and 24 h, respectively, before they were used to conduct disinfection experiments on fresh *S. aureus* cells in the dark under the same experimental setup as the photocatalytic disinfection experiment only without the light illumination. Figure 4b shows the *S. aureus* cell survival ratios in the dark treated by pre-illuminated Cu_2O/SnO_2 samples after being stored in the dark for various times. It demonstrated clearly that pre-illuminated Cu_2O/SnO_2 samples could effectively disinfect *S. aureus* cells in the dark even after the visible illumination was shut off. When the dark storage time was 0 h, the survival ratio of *S. aureus* cells dropped to ~0.9% after only 35 min treatment in dark. With the increase of the dark storage time from 3 h, 8 h, to 24 h, the bactericidal effect of the pre-illuminated Cu_2O/SnO_2 sample in the dark dropped gradually, and the survival ratio of *S. aureus* cells after 35 min treatment in dark increased from ~2.4%, ~11.9%, to ~44.5%, respectively. In the dark, the survival ratio curve of *S. aureus* cells treated by the pre-illuminated Cu_2O/SnO_2 sample with the dark storage time of 24 h was close to that treated by the same photocatalyst without pre-illumination. This observation clearly demonstrated that the post-illumination disinfection capability of the Cu_2O/SnO_2 sample in the dark relied on its "memory" of the visible light illumination prior to the dark environment, not the photocatalytic material itself. The observed post-illumination photocatalytic "memory" effect in the dark of SnO_2 nanoparticle-decorated Cu_2O nanocubes with pre-illumination was stronger than that of TiON/PdO and Cu_2O-NS/TiO_2-NI photocatalysts developed in our previous work[14–16]. In these photocatalytic material systems, electron trapping and release occurred when the visible light illumination was on and off, respectively, which enhanced their photocatalytic performances under visible light illumination and resulted in their post-illumination photocatalytic "memory" in the dark.

The production and role of H_2O_2 in the photocatalytic disinfection under visible light illumination and post-illumination photocatalytic "memory" disinfection in the dark of *Staphylococcus aureus* bacteria. Generally, various reactive oxygen species, such as H_2O_2, $^{\bullet}O_2^-$, $^{\bullet}OH$, h^+, and e^-, are produced *in situ* during the photocatalytic process[37]. To verify the occurrence of the two-electron reduction of O_2 to H_2O_2 by the Cu_2O/SnO_2 sample, the concentrations of H_2O_2 in the test solution were examined by a colorimetric DPD method under visible light illumination and in the dark, respectively. Figure 5a shows the H_2O_2 concentrations in the test solution under visible light illumination by the Cu_2O/SnO_2 sample, the as-synthesized Cu_2O nanocubes, and SnO_2 nanoparticles, respectively. It demonstrated that the H_2O_2 yield increased at first and then became relatively stable with prolonged illumination time because the consumption of H_2O_2 was in parallel with its production, which gradually reached the equilibrium. The H_2O_2 production by the Cu_2O/SnO_2 sample was much higher than Cu_2O nanocubes and SnO_2 nanoparticles. The measured equilibrium H_2O_2 concentration was ~2.33 μM for the Cu_2O/SnO_2 sample, ~772% as that of SnO_2 nanoparticles and ~438% as that of the Cu_2O nanocubes. The observed enhancement of H_2O_2 production could be attributed to the transfer of photogenerated electrons from Cu_2O to SnO_2 under visible light illumination due to the formation of Cu_2O/SnO_2 *p-n* heterojunction, which in turn could enhance photogenerated electron-hole pair separation in Cu_2O and increase the production of $^{\bullet}OH$ because more holes on the valence band of Cu_2O could have the chance to migrate to the surface of Cu_2O and react with H_2O to form $^{\bullet}OH$. Thus, the Cu_2O/SnO_2 sample demonstrated much better photocatalytic performances on the degradation of SMX and disinfection of *S. aureus* cells than Cu_2O nanocubes under visible light illumination. It must be pointed out that the total amount of H_2O_2 produced should be much higher than the measured equilibrium concentration value because it was consumed *in situ* in the system with its generation.

Figure 5b shows the H_2O_2 concentrations in the test solution in the dark for an extended period of time up to 24 h after the visible light illumination was turned off by the Cu_2O/SnO_2 sample, the as-synthesized Cu_2O nanocubes, and SnO_2 nanoparticles, respectively. For the as-synthesized Cu_2O nanocubes and SnO_2 nanoparticles, their production of H_2O_2 was limited and the H_2O_2 concentrations dropped quickly within the first 30 min in the dark. This observation was similar to the previous reports on Se[17] and Bi[18], in which very limited charge carriers could remain at their surfaces, produce ROSs after the illumination was shut off, and be consumed quickly. After 30 min, the equilibrium H_2O_2 concentrations was ~0.33 μM for Cu_2O nanocubes and ~0.25 μM for SnO_2

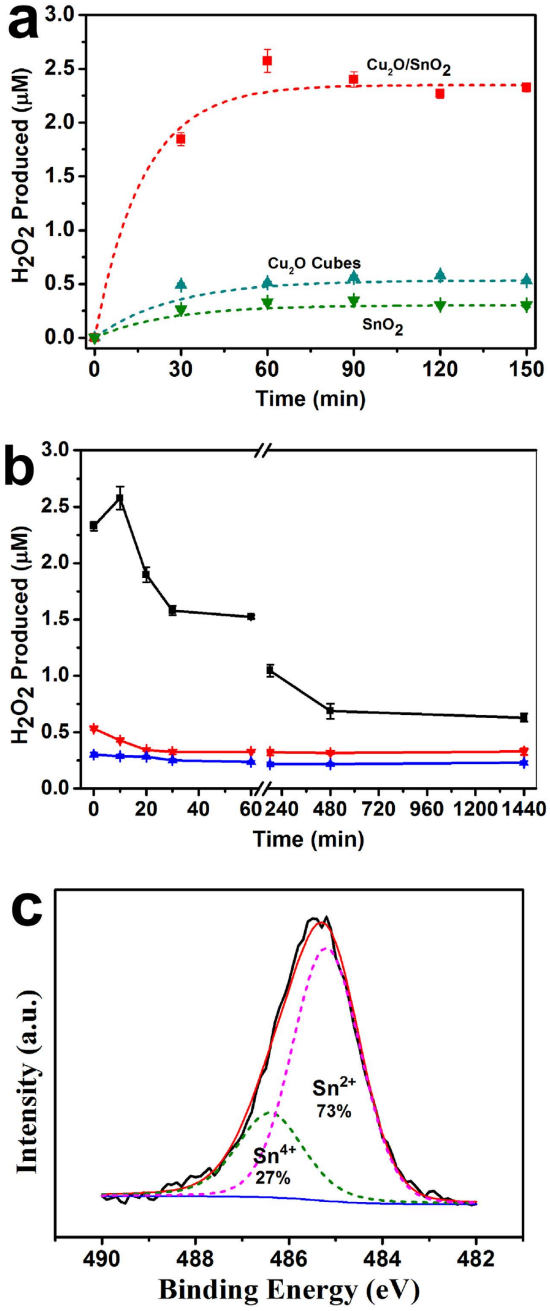

Figure 5. The H_2O_2 concentrations in the test solution by the Cu_2O/SnO_2 sample, the as-synthesized Cu_2O nanocubes, and SnO_2 nanoparticles, respectively: (**a**) under visible light illumination, and (**b**) in the dark for up to 24 h after being illuminated under visible light for 3 h. (**c**) The high resolution XPS scan over Sn *3d* peaks under visible light illumination.

nanoparticles for the whole experiment time up to 24 h in the dark, which may reflect the H_2O_2 concentration in the environment background. For the Cu_2O/SnO_2 sample, however, a completely different H_2O_2 production behavior was observed. The H_2O_2 concentration increased quickly for the first 10 min in the dark, which could be attributed to the quick release of trapped electrons from SnO_2 to react with O_2. Then, it decreased gradually afterwards up to 24 h in the dark as long as the experiment explored. Even after 24 h in the dark, the H_2O_2 concentration still reached ~0.63 μM, much higher than the H_2O_2 concentration in the environment background. Thus, the Cu_2O/SnO_2 sample could still be active to disinfect *S. aureus* cells in the dark even after the light illumination was off for 24 h as shown in Fig. 4b. The gradual decrease of the H_2O_2 concentration with the increase of dark time also clearly demonstrated that the post-illumination disinfection capability of the Cu_2O/SnO_2 sample in the dark relied on its "memory" of the visible light illumination prior to the dark environment, which was the trapping of photogenerated electrons.

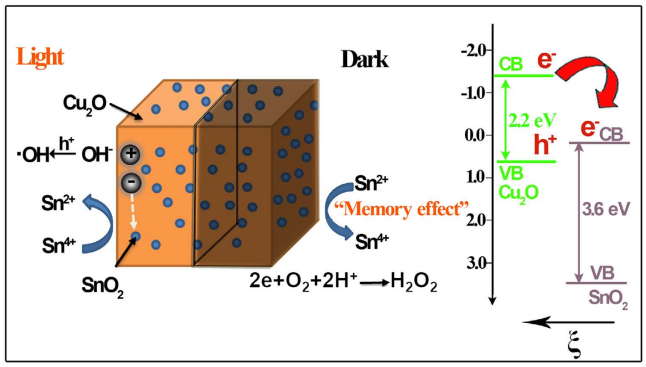

Figure 6. The proposed energy band structure of the Cu_2O/SnO_2 *p-n* heterojunction, the photocatalytic activity enhancement mechanism under visible light illumination, and the post-illumination photocatalytic "memory" mechanism in the dark.

Figure 5c shows the high resolution XPS scan over Sn *3d* peaks under visible light illumination. The Sn^{4+}/Sn^{2+} ratio was determined to be ~27:73. Compared to that without illumination as shown in Fig. 2d, a large part of Sn^{4+} was reduced to Sn^{2+}, which came from the transfer of photogenerated electrons from Cu_2O to SnO_2 under visible light illumination and the subsequent trapping of part of these electrons by SnO_2. After the light illumination was shut off, these trapped electrons could be gradually released and react with O_2 to produce H_2O_2 as shown in Fig. 5b. To further confirm the production of H_2O_2 and its major contribution to the disinfection of *S. aureus* cells by the Cu_2O/SnO_2 sample in the dark after the illumination was shut off, a H_2O_2 scavenger, EDTA-Fe(II), was used to examine if its existence could affect the survival ratio of *S. aureus* cells[38]. 0.1 mM EDTA-Fe(II) was added into the *S. aureus* cell suspension, and the pre-illuminated Cu_2O/SnO_2 sample was used to conduct the disinfection experiment in the dark. As shown in Fig. 5b, the presence of EDTA-Fe(II) largely enhanced the survival ratio of *S. aureus* cells, which was very close to that treated by the Cu_2O/SnO_2 sample without pre-illumination in the dark. This observation further confirmed that H_2O_2 was the dominant ROS involved in the photocatalytic "memory" disinfection of *S. aureus* cells by the pre-illuminated Cu_2O/SnO_2 sample in the dark.

Discussion

Figure 6 shows the proposed energy band structure of the Cu_2O/SnO_2 *p-n* heterojunction, the photocatalytic activity enhancement mechanism under visible light illumination[39,40], and the post-illumination photocatalytic "memory" mechanism in the dark. When *p*-type Cu_2O and *n*-type SnO_2 formed a heterojunction, charge carrier concentration gradient occurred at the interface. Thus, the diffusion of electrons from SnO_2 to Cu_2O and the diffusion of holes with the opposite direction happened until reaching the equilibrium, and an inner electric field (ξ) was built at the interface as demonstrated in Fig. 6. Under visible light illumination, only Cu_2O was excited to produce electron-hole pairs. The combined effect from both the large conduction band potential difference (~1.5 eV) and the inner electric field (ξ) provided a strong driving force for photogenerated electrons to transfer from the conduction band of Cu_2O to that of SnO_2 and be trapped there as verified by experimental evidences of the H_2O_2 production and XPS analysis on Sn chemical status change from Sn^{4+} to Sn^{2+}. Thus, the photogenerated electron-hole pairs were separated effectively, and a largely enhanced photocatalytic performance was observed on the Cu_2O/SnO_2 sample for its degradation of SMX and disinfection of *S. aureus* cells, compared with pure Cu_2O nanocubes, which was very similar to our previous report on Cu_2O-NS/TiO_2-NI photocatalyst system[16]. When the visible light illumination was shut off, the trapped electrons could be released from SnO_2 and the two-electron reduction of O_2 could happen by its reaction with these released electrons due to their matched reduction potentials, which was verified by the continuous production of H_2O_2 in the dark for more than 24 h. So the Cu_2O/SnO_2 sample could demonstrate the post-illumination photocatalytic "memory" disinfection of *S. aureus* cells in the dark after the illumination was shut off.

The ROS production in the dark by the Cu_2O/SnO_2 sample developed in this study was quite different with that of previous reported photocatalysts with the post-illumination photocatalytic "memory" effect[14–16,19]. For TiON/PdO[14,15], Cu_2O-NS/TiO_2-NI[16], and I-TiO_2[19], photogenerated electrons were released from the decoration components in the dark and one-electron reduction of O_2 happened to produce $^{\bullet}O_2^-$ and subsequently $^{\bullet}OH$ as ROSs, which required the decoration components had the conduction band potential negative than the one-electron reduction potential of O_2. For the Cu_2O/SnO_2 sample, however, photogenerated electrons were released from SnO_2 in the dark and two-electron reduction of O_2 happened to produce H_2O_2 as ROS. Thus, this work demonstrated that a decoration component with the conduction band potential less positive than the two-electron reduction potential of O_2 could also be effective to generate the post-illumination photocatalytic "memory" effect from the production of H_2O_2 in the dark.

This finding suggested that the selection of potential decoration components to construct photocatalyst systems with the post-illumination photocatalytic "memory" effect could be largely expanded to more semiconductors, such as SnO_2, WO_3, $CuWO_4$, $BiWO_6$, CeO_2, etc. Although they do not have conduction band potentials negative than the one-electron reduction potential of O_2, so trapped electrons released by them could not reduce O_2 in the dark to produce $^{\bullet}O_2^-$ and subsequently $^{\bullet}OH$. However, electrons trapped on them could be released and then reduce O_2 in the dark to produce the reactive oxygen species of H_2O_2 because their conduction band

potentials are less positive than the two-electron reduction potential of O_2. Thus, novel photocatalyst systems with the post-illumination photocatalytic "memory" effect could be designed based on these decoration components paired with light absorber components of proper conduction band potentials in which photogenerated electrons could transfer from the light absorber component to the decoration component for subsequent trapping under light illumination and release after the illumination was shut off. Furthermore, different photocatalyst systems with the post-illumination photocatalytic "memory" effect could be designed by modulating the conduction band potential of the decoration component to produce different kinds of ROSs for the optimized performance for various applications.

In summary, a novel composite photocatalyst composed of Cu_2O nanocubes decorated with SnO_2 nanoparticles was successfully created, in which Cu_2O served as the main visible light absorber, while SnO_2 nanoparticle decoration formed *p-n* heterojunction of good contact with Cu_2O nanocubes. The combined effect from both their large conduction band potential difference and the inner electric field provided a strong driving force for photogenerated electrons to transfer from the conduction band of Cu_2O to that of SnO_2 and be trapped there under visible light illumination. Thus, a largely enhanced photocatalytic performance was observed on these Cu_2O/SnO_2 photocatalysts as demonstrated by its disinfection of *S. aureus* cells and degradation of SMX, compared with pure Cu_2O nanocubes. When the visible light illumination was turned off, trapped electrons could be released from SnO_2 and react with O_2 to produce H_2O_2 in the dark for more than 24 h, and the Cu_2O/SnO_2 sample demonstrated a strong post-illumination photocatalytic "memory" disinfection of *S. aureus* cells in the dark. This work demonstrated that the selection of potential decoration components to construct photocatalyst systems with the post-illumination photocatalytic "memory" effect could be largely expanded to semiconductors with conduction band potentials less positive than the two-electron reduction potential of O_2. With high efficiency and relatively low cost/energy consumption, photocatalysts with the post-illumination photocatalytic "memory" effect could have the potential for a broad range of environmental applications which require the continuous activity in the dark for an extended period of time.

Methods

Chemicals and materials. Copper(II) chloride dihydrate ($CuCl_2 \cdot 2H_2O$, 99%, Sinopharm Chemical Reagent Co., Ltd., Shanghai, P. R. China) was used as the Cu source, polyvinylpyrrolidon (PVP k30, Sinopharm Chemical Reagent Co., Ltd., Shanghai, P. R. China) was used as the surfactant, sodium hydroxide (NaOH, 96%, Sinopharm Chemical Reagent Co., Ltd., Shanghai, P. R. China) was used as the precipitation reagent, and L-ascorbic acid (99.7%, Aladdin Industrial Corporation Co. Ltd., Shanghai, P. R. China) was used as the reducing agent in the synthesis of Cu_2O nanocubes, respectively. Deionized (DI) water was used as the solvent in this process. Potassium stannate trihydrate ($K_2SnO_3 \cdot 3H_2O$, 99.5%, Aladdin Industrial Corporation Co. Ltd., Shanghai, P. R. China) was used as the Sn source and Ethyl acetate ($C_4H_8O_2$, 99.5%, Sinopharm Chemical Reagent Co., Ltd., Shanghai, P. R. China) was used as the hydrolytic reagent in the formation of SnO_2 nanoparticles. Sulfamethoxazole (SMX, 98%, Aladdin Industrial Corporation Co. Ltd., Shanghai, P. R. China) was used as the target organic pollution compound for the investigation of the sample's visible light-induced photocatalytic activity. Sodium diethydlthiocabamate (DDTC, 99%, Sinopharm Chemical Reagent Co., Ltd., Shanghai, P. R. China) was used to detect the Cu^{2+}concentration. Horseradish peroxide (POD,>200 units/mg, Aladdin Industrial Corporation Co. Ltd., Shanghai, P. R. China) and N,N-diethyl-p-phenylenediamine sulfate (DPD, 98% , Aladdin Industrial Corporation Co. Ltd., Shanghai, P. R. China) were used as the chromogenic reagents, while phenol (99%, Alfa Aesar Chemical Ltd., Tianjin, P. R. China) was used as the hole scavenger in the detection of the H_2O_2 concentration experiment.

Synthesis of Cu_2O nanocubes. Cu_2O nanocubes were synthesized by a modified process based on a previous report[41]. In a typical experiment, 0.3 g PVP was first dissolved in 270 mL DI water, and 30 mL of 0.02 M $CuCl_2 \cdot 2H_2O$ solution was added into the PVP solution. Then, 3.6 mL of 0.6 M NaOH was added drop wise (1 drop/s) into the above mixture solution with continual stirring. Finally, 4 mL of 0.3 M L-ascorbic acid was added drop wise into the mixture solution and it was further stirred for 5 min before being centrifuged at 9,500 rpm for 5 min. All of these procedures were carried out in a water bath at 35 °C. The obtained yellow precipitates were washed with excessive DI water and ethanol for several times to remove unreacted chemicals and PVP surfactants.

Preparation of SnO_2 nanoparticle-decorated Cu_2O nanocubes. The obtained Cu_2O nanocubes were dispersed in a mixture solvent consisting of 15 mL of DI water and 10 mL of absolute ethanol with the aid of ultrasonication for 15 min. Then, 2.5 mL of 0.01 M potassium stannate trihydrate ($K_2SnO_3 \cdot 3H_2O$) solution was slowly dropped into the Cu_2O suspension and stirred for 10 min. After thorough mixing, 0.2 mL of ethyl acetate ($C_4H_8O_2$) was added drop wise into the mixture under vigorous stirring for 1 h. Finally, the suspension was transferred into a 50 mL Teflon-lined stainless steel autoclave, and heated at 170 °C for 6 h in an oven. After the reaction, the products were collected, went through several rinse-centrifugation cycles with DI water and ethanol separately, and then dried at 40 °C for 12 h in a vacuum oven. Bare SnO_2 nanoparticles were also prepared via the same hydrothermal process without the adding of Cu_2O nanocubes and were used as a reference material for the photocatalytic testing.

Materials characterization. The crystal structures of the as-prepared samples were analyzed by X-ray diffraction (XRD) on a D/MAX-2004 X-ray powder diffractometer (Rigaku Corporation, Tokyo, Japan) with Ni-filtered Cu Kα ($\lambda = 1.54178$ Å) radiation at 56 kV and 182 mA. The morphologies of the as-prepared samples were observed by the transmission electron microscopy (TEM). TEM observations were conducted on a JEOL 2100 TEM (JEOL Ltd., Tokyo, Japan) operated at 200 kV with point-to-point resolution of 0.28 nm, and TEM samples were prepared by dispersing a thin film of these powder samples on Ni grids. A Tecnai G2

F20 transmission electron microscope (FEI, Acht, The Netherlands) was used to obtain high-resolution TEM (HRTEM) images of samples. X-ray photoelectron spectroscopy (XPS) measurements were conducted using an ESCALAB 250 X-ray photoelectron spectrometer (Thermo Fisher Scientific Inc., Waltham, MA, U. S. A.) with an Al Kα anode (1486.6 eV photon energy, 300 W). The UV-vis spectra of samples and concentration of SMX were measured on a UV-2550 spectrophotometer (Shimadzu Corporation, Kyoto, Japan).

Photocatalytic disinfection of Staphylococcus aureus (*S. aureus*) bacteria under visible light illumination. Wild-type *S. aureus* (CMCC(B)26003, China national standard material network, P. R. China) were used for photocatalytic disinfection experiments. After overnight culture, cells were diluted to a cell suspension (ca.10^7 cfu/mL) in 0.9% NaCl solution prior to the use for photocatalytic disinfection experiments. All solid or liquid materials had been autoclaved for 30 min at 121 °C before use. The same visible light source was used as in the photocatalytic degradation of SMX. In the photocatalytic disinfection of *S. aureus* bacteria experiment, aliquot of 10 mL *S. aureus* cell suspension was pipetted onto a sterile 50 × 10 mm petri dish with the photocatalytst sample, which was first spin coated at the bottom of the dish. A fixed concentration of ~0.2 mg photocatalyst/mL *S. aureus* solution was used in this experiment. At regular time intervals, 100 μL of aliquots of the powder-treated cell suspensions were withdrawn in sequence. After appropriate dilutions in 0.9% NaCl solution, aliquot of 100 μL was spread onto an agar medium plate and incubated at 37 °C for 15 h. The number of viable cells in terms of colony-forming units was counted. Tests were also performed in the dark in the presence of the photocatalyst for comparison. Analyses were in triplicate, and control runs were carried out each time under the same experiment conditions, but without any photocatalytic materials.

Photocatalytic "memory" disinfection of Staphylococcus aureus (*S. aureus*) bacteria in the dark. For *S. aureus* bacteria disinfection under dark environment, the Cu_2O/SnO_2 sample was firstly illuminated by the same lamp for ~3 h. Then, the lamp was shut off and they were used to conduct disinfection experiments in the dark over fresh *S. aureus* cell suspensions (ca. 10^7 cfu/mL) either immediately or after being kept in dark for 3, 8 and 24 h. In some experiments, Fe(II)-EDTA (0.1 mM) was added for the removal of H_2O_2 to examine the reactive oxygen species[37,38]. All experimental conditions were the same as that for the photocatalytic disinfection of *S. aureus* bacteria, but without the visible light illumination.

Detection of the hydrogen peroxide (H_2O_2) concentration. The colorimetric DPD method based on the horseradish peroxidase (POD) catalyzed oxidation of *N*,*N*-diethyl-*p*-phenylenediamine (DPD) was used for the detection of *in situ* photogenerated H_2O_2[42]. 0.1 g *N*,*N*-diethyl-*p*-phenylenediammonium sulfate was first dissolved in 10 mL of 0.1 M H_2SO_4 solution, and 10 mg POD was dissolved in 10 mL DI water. Both DPD and POD solutions were stored in the dark at 4 °C in a refrigerator and replaced with fresh solutions at weekly intervals. For the detection of H_2O_2 concentration, 5 mL aliquot of the test solution was pipetted into a 10 mL test tube, and mixed with 0.5 mL phosphate buffer solution (0.5 M KH_2PO_4 and 0.5 M K_2HPO_4) to yield a pH of ~6.0. 50 μL DPD solution was then added into the mixture solution, followed by the addition of 50 μL POD solution with shaking for 10 sec. The solution was then settled for 30 sec before the UV-vis spectrum measurement. The H_2O_2 concentration could be quantified by the UV-2550 spectrophotometer monitoring the absorption maximum at λ_{max} of 551 nm.

References

1. Rawalekar, S. & Mokari, T. Rational design of hybrid nanostructures for advanced photocatalysis. *Adv. Energy Mater.* **3,** 12–27 (2013).
2. Hoffmann, M. R., Martin, S. T., Choi, W. & Bahnemann, D. W. Environmental applications of semiconductor photocatalysis. *Chem. Rev.* **95,** 69–96 (1995).
3. Liu, J. *et al.* Metal-free efficient photocatalyst for stable visible water splitting via a two-electron pathway. *Science* **347,** 970–974 (2015).
4. Li, L. D. *et al.* Sub-10 nm rutile titanium dioxide nanoparticles for efficient visible-light-driven photocatalytic hydrogen production. *Nat. Commun.* **6,** 5881 (2015).
5. Mi, Y. & Weng, Y. Band alignment and controllable electron migration between rutile and anatase TiO_2. *Sci. Rep.* **5,** 11482 (2015).
6. Jia, H. *et al.* Generation of reactive oxygen species, electrons/holes, and photocatalytic degradation of Rhodamine B by photoexcited CdS and Ag_2S Micro-Nano Structures. *J. Phys. Chem. C* **118,** 21447–21456 (2014).
7. George, S. *et al.* Role of Fe doping in tuning the band gap of TiO_2 for the photo-oxidation-induced cytotoxicity paradigm. *J. Am. Chem. Soc.* **133,** 11270–11278 (2011).
8. Sheng, J., Li, X. & Xu, Y. Generation of H_2O_2 and OH radicals on Bi_2WO_6 for phenol degradation under visible Light. *ACS Catal.* **4,** 732–737 (2014).
9. Zhang, J., Liu, Y., Li, Q., Zhang, X. & Shang, J. K. Antifungal activity and mechanism of palladium-modified nitrogen-doped titanium oxide photocatalyst on agricultural pathogenic fungi Fusarium graminearum. *ACS Appl. Mater. Interface* **5,** 10953–10959 (2013).
10. Li, R. *et al.* Spatial separation of photogenerated electrons and holes among {010} and {110} crystal facets of $BiVO_4$. *Nat. Commun.* **4,** 1432 (2012).
11. Wang, H. *et al.* Semiconductor heterojunction photocatalysts: design, construction, and photocatalytic performances. *Chem. Soc. Rev.* **43,** 5234–5244 (2014).
12. Tilmaciu, C. M. *et al. In vitro* and *in vivo* characterization of antibacterial activity and biocompatibility: a study on silver-containing phosphonate monolayers on titanium. *Acta Biomater.* **15,** 266–277 (2015).
13. Zollfrank, C., Gutbrod, K., Wechsler, P. & Guggenbichler, J. P. Antimicrobial activity of transition metal acid MoO_3 prevents microbial growth on material surfaces.*Mater. Sci. Eng. C Mater. Biol. Appl.* **32,** 47–54 (2012).
14. Li, Q., Li, Y. W., Wu, P., Xie, R. & Shang, J. K. Palladium oxide nanoparticles on nitrogen-doped titanium oxide: accelerated photocatalytic disinfection and post-illumination catalytic "memory". *Adv. Mater.* **20,** 3717–3723 (2008).
15. Li, Q., Li, Y. W., Liu, Z., Xie, R. & Shang, J. K. Memory antibacterial effect from photoelectron transfer between nanoparticles and visible light photocatalyst. *J. Mater. Chem.* **20,** 1068–1072 (2010).

16. Liu, L., Yang, W., Li, Q., Gao, S. & Shang, J. K. Synthesis of Cu_2O nanospheres decorated with TiO_2 nanoislands, their enhanced photoactivity and stability under visible light illumination, and their post-illumination catalytic memory. *ACS Appl. Mater. Interfaces* **6,** 5629–5639 (2014).
17. Chiou, Y. D. & Hsu, Y. J. Room-temperature synthesis of single-crystalline Se nanorods with remarkable photocatalytic properties. *Appl. Catal. B-Environ.* **105,** 211–219 (2011).
18. Dong, F. *et al.* A semimetal bismuth element as a direct plasmonic photocatalyst. *Chem. Commun.* **50,** 10386–10389 (2014).
19. Lin, H. *et al.* Iodine-modified nanocrystalline titania for photocatalytic antibacterial application under visible light illumination. *Appl. Catal. B-Environ.* **176-177,** 36–43 (2015).
20. Liu, G. *et al.* Band-to-band visible-light photon excitation and photoactivity induced by homogeneous nitrogen doping in layered titanates. *Chem. Mater.* **21,** 1266–1274 (2009).
21. Zhu, L. *et al.* Hierarchical assembly of SnO_2/ZnO nanostructures for enhanced photocatalytic performance. *Sci. Rep.* **5,** 11609 (2015).
22. Batzill, M. & Diebold, U. The surface and materials science of tin oxide. *Prog. Surf. Sci.* **79,** 47–154 (2005).
23. Tian, Q. *et al.* Tube-like ternary α-Fe_2O_3@SnO_2@Cu_2O sandwich heterostructures: synthesis and enhanced photocatalytic properties. *ACS Appl. Mater. Interfaces* **6,** 13088–13097 (2014).
24. Bai, S. *et al.* A unique semiconductor-metal-graphene stack design to harness charge flow for photocatalysis. *Adv. Mater.* **26,** 5689–5695 (2014).
25. Liu, L., Yang, W., Sun, W., Li, Q. & Shang, J. K. Creation of Cu_2O@TiO_2 composite photocatalysts with p-n heterojunctions formed on exposed Cu_2O facets, their energy band alignment study, and their enhanced photocatalytic activity under illumination with visible light. *ACS Appl. Mater. Interfaces* **7,** 1465–1476 (2015).
26. Yin, M. *et al.* Copper oxide nanocrystals. *J. Am. Chem. Soc.* **127,** 9506–9511 (2005).
27. Ghijsen, J. *et al.* Electronic structure of Cu_2O and CuO. *Phys. Rev. B* **38,** 11322–11330 (1988).
28. Yang, D. J., Kamienchick, I., Youn, D. Y., Rothschild, A. & Kim, I.D. Ultrasensitive and highly selective gas sensors based on electrospun SnO_2 nanofibers modified by Pd loading. *Adv. Funct. Mater.* **20,** 4258–4264 (2010).
29. Fan, C. M. *et al.* Synproportionation reaction for the fabrication of Sn^{2+} self-doped SnO_{2-x} nanocrystals with tunable band structure and highly efficient visible light photocatalytic activity. *J. Phys. Chem. C* **117,** 24157–24166 (2013).
30. Tauc, J., Grigorovici, R. & Vancu, A. Optical properties and electronic structure of amorphous germanium. *phys. status solidi (b)* **15,** 627–637 (1966).
31. Ng, C. H. B. & Fan, W. Y. Shape evolution of Cu_2O nanostructures via kinetic and thermodynamic controlled growth. *J. Phys. Chem. B* **110,** 20801–20807 (2006).
32. Kuo, C., Chen, C. & Huang, M. H. Seed-mediated synthesis of monodispersed Cu_2O nanocubes with five different size ranges from 40 to 420 nm. *Adv. Funct. Mater.* **17,** 3773–3780 (2007).
33. Ahmad, E. K. *et al.* Controlling core/shell formation of nanocubic p-Cu_2O/n-ZnO toward enhanced photocatalytic performance. *Langmuir* **31,** 10922–10930 (2015).
34. Liu, L. *et al. In situ* loading of ultra-small Cu_2O particles on TiO_2 nanosheets to enhance the visible-light photoactivity. *Nanoscale* **4,** 6351–6359 (2012).
35. Uddin, M. T. *et al.* Nanostructured SnO_2-ZnO heterojunction photocatalysts showing enhanced photocatalytic activity for the degradation of organic dyes. *Inorg. Chem.* **51,** 7764–7473 (2012).
36. Giannousi, K., Lafazanis, K., Arvanitidis, J., Pantazaki, A. & Dendrinou-Samara, C. Hydrothermal synthesis of copper based nanoparticles: antimicrobial screening and interaction with DNA. *J Inorg. Biochem.* **133,** 24–32 (2014).
37. Shi, H. *et al.* Role of *in situ* resultant H_2O_2 in the visible-light-driven photocatalytic inactivation of *E. coli* using natural sphalerite: a genetic study. *J. Phys. Chem. B* **119,** 3104–3111 (2015).
38. Khachatryan, L., Vejerano, E., Lomnicki, S. & Dellinger, B. Environmentally persistent free radicals (EPFRs). 1. Generation of reactive oxygen species in aqueous solutions. *Environ. Sci. Technol.* **45,** 8559–8566 (2011).
39. Yang, L. *et al.* High efficient photocatalytic degradation of p-Nitrophenol on a unique Cu_2O/TiO_2 *p-n* heterojunction network catalyst. *Environ. Sci. Technol.* **44,** 7641–7646 (2010).
40. Hou, Y., Li, X. Y., Zhao, Q. D., Quan, X. & Chen, G. H. Fabrication of Cu_2O/TiO_2 nanotube heterojunction arrays and investigation of its photoelectrochemical behavior. *Appl. Phys. Lett.* **95,** 093108 (2009).
41. Yec, C. C. & Zeng, H. C. Synthetic architecture of multiple core–shell and yolk–shell structures of $(Cu_2O@)_nCu_2O$ (n = 1–4) with centricity and eccentricity. *Chem. Mater.* **24,** 1917–1929 (2012).
42. Bader, H., Sturzenegger, V. & Hoigné, J. Photometric method for the determination of low concentrations of hydrogen peroxide by the peroxidase catalyzed oxidation of N,N-diethyl-p-phenylenediamine (DPD). *Water Res.* **22,** 1109–1115 (1988).

Acknowledgements

This study was supported by the National Natural Science Foundation of China (Grant No. 51102246), the Youth Innovation Promotion Association, Chinese Academy of Sciences (Grant No. Y2N5711171), and the Basic Science Innovation Program of Shenyang National Laboratory for Materials Science (Grant No. Y4N56R1161).

Author Contributions

Q.L. initiated and supervised all of the work and prepared the manuscript. L.L. carried out the experiments and contributed to drafting the manuscript. W.S. developed the approach to decorate SnO_2 nanoparticles onto Cu_2O nanocubes. W.Y. and J.K.S. revised the manuscript.

Additional Information

Supplementary information accompanies this paper at http://www.nature.com/srep

Competing financial interests: The authors declare no competing financial interests.

How to cite this article: Liu, L. *et al.* Post-illumination activity of SnO_2 nanoparticle-decorated Cu_2O nanocubes by H_2O_2 production in dark from photocatalytic "memory". *Sci. Rep.* **6**, 20878; doi: 10.1038/srep20878 (2016).

This work is licensed under a Creative Commons Attribution 4.0 International License. The images or other third party material in this article are included in the article's Creative Commons license, unless indicated otherwise in the credit line; if the material is not included under the Creative Commons license, users will need to obtain permission from the license holder to reproduce the material. To view a copy of this license, visit http://creativecommons.org/licenses/by/4.0/